Hindawi Publishing Corporation
International Journal of Photoenergy
Volume 2011, Article ID 518153, 10 pages
doi:10.1155/2011/518153

Research Article

Heterogeneous Photodecolorization of Methyl Green Catalyzed by Fe(II)-*o*-Phenanthroline/Zeolite Y Nanocluster

Alireza Nezamzadeh-Ejhieh and Elahe Shahriari

Department of Chemistry, Shahreza Branch, Islamic Azad University, P.O. Box 311-86145, Shahreza, Isfahan, Iran

Correspondence should be addressed to Alireza Nezamzadeh-Ejhieh, arnezamzadeh@iaush.ac.ir

Received 4 June 2011; Revised 3 August 2011; Accepted 25 August 2011

Academic Editor: M. S. Abdel-Mottaleb

The potential of Fe(II)-orthophenatrolin, as doped with synthetic zeolite Y nanocluster (Na-Y) via complexation process, after wet impregnation of parent zeolite with $FeSO_4$ aqueous solution, was studied as a photocatalyst in decolorization of Methyl Green (MG) under UV irradiation. The characterization of the synthesized zeolite nanocluster and the prepared catalyst was studied using X-ray powder diffraction (XRD), infrared spectroscopy (FT-IR), thermal analysis, and SEM methods. The dye photodecolorization process was studied considering the influence of experimental parameters and it was observed that photoreactivity of the photocatalyst was varied with catalyst amount, initial dye concentration, pH of dye solution, temperature, and the presence of $KBrO_3$. The optimal experimental parameters were obtained as follows: catalyst amount: 1 gL^{-1}, dye concentration: 40 ppm, pH: 9, and active component value: 100 mg Fe(II)-orthophenatrolin per g catalyst. The reusability of the intended catalyst was also investigated. The degradation process obeyed first-order kinetics.

1. Introduction

From an ecological and physiological point of view, the elimination of toxic chemicals from wastewaters is currently one of the most important subjects in pollution control. Triphenylmethane dyes are used extensively in the textile industry for dyeing of nylon, wool, cotton, and silk, as well as for coloring of oil, fats, waxes, varnish, and plastics. The paper, leather, cosmetic, and food industries consume a high quantity of various kinds of triphenylmethane dyes [1]. Cationic triphenylmethane dyes are widely used as colorants and antimicrobial agents in different industries [2]. Previous reports indicate that they may further serve as targetable sensitizers in the photodestruction of specific cellular components or cells [3]. Methyl green (MG) is a basic triphenylmethane and dicationic dye usually used for staining of solutions in medicine and biology [4]. It is also used as a photochromophore to sensitize gelatinous films [5].

The growing interest in the development of new methodologies for the degradation of toxic water pollutants has led to conclude that the most effective way for oxidation of organic pollutants can be achieved when a powerful oxidizing agent, especially a free-radical-like $^{\bullet}OH$, is generated [6, 7].

Recently supporting of semiconductors by various supports has been widely investigated. Among the supports, zeolites have more advantageous owing to their special features such as high surface area, hydrophobic and hydrophilic properties, tunable chemical properties, high thermal stability, and eco-friendly nature. Zeolites are microporous microcrystalline inorganic materials capable of adsorbing organic molecules [8, 9]. They possess regular periodic structures with channels and cages extending regularly all over their structures. Adsorption of organic guest molecules may occur both on the external and on internal surfaces of a zeolite crystal. Normally, molecular alignment and conformational restrictions occur on guest molecules, which are particularly effective in zeolites photoactivity. In recent years, zeolites modified with transition metal complex have received increasing attention as promising catalysts for a variety of important reactions [10]. The easiness in change of their oxidation state makes the transition metal ions responsible for most redox processes occurring in nature directly or via a catalytic mechanism. The chemically inert complexes of

metal ions in their higher oxidation state, as Fe(III) and Cu(II), undergo readily photoreduction to Fe(II) and Cu(I), respectively, which is accompanied by oxidation of the organic ligand, or other sacrificial donors. Thus, the environmental photochemistry of the transition metal complexes with organic ligands has a crucial importance for the pollution abatement because it may cause the photodegradation of persistent pollutants, such as phenol and its derivatives or EDTA and related aminopolycarboxylic acids [11, 12]. The mechanism of the photocatalysis by the transition metal complexes in a homogeneous phase has been described in [13].

Generally, the environmental Fe compounds are classified into two groups, the hydroxo species and chelate complexes, depending on the nature of their ligand oxidation products [14]. The inner- and outer-sphere photoinduced electron transfer mechanisms have been reported for Fe^{3+} complexes, that cause producing of $^{\bullet}OH$ and $^{\bullet}X$ (X^- is the oxidizable ions or molecules present in the vicinity of the catalyst such as Cl^-Br^- and SCN^-), respectively [15–17].

In the present study, nanocluster of zeolite Y was synthesized and characterized with FT-IR, XRD, thermal methods, and SEM. The zeolite was exchanged with Fe(II) solution. Then Fe(II)-o-phenanthroline/zeolite Y nano cluster (FOZYNC) photocatalyst was prepared. The activity of the obtained photocatalyst was evaluated by studying the photocatalytic decolorization of methyl green. The effects of catalyst dosage, methyl green concentration, pH, and temperature were studied as functions of percentage of decolorization under UV irradiation. For the sake of comparison, corresponding dark controls were also carried out.

2. Experimental

2.1. Chemicals. MG dye (molecular formula: $C_{27}H_{35}Cl_2N_3$) and Ortho-phenanthroline ($C_{12}H_8N_2 \cdot H_2O$) were purchased from Merck. Sodium silicate was the product of Merck and its composition is SiO_2 (25.2–28.5%), Na_2O (7.5–8.5%), and H_2O (63%). Iron(II) sulphate, hydrochloric acid (37%), sulfuric acid (98%), sodium hydroxide (98%), tetrapropylammonium bromide (TPABr 98%), aluminum sulfate eighteenhydrate (>99.3%), sodium chloride (99.5%) were supplied from Merck. Deionized water was used throughout the experiments.

2.2. Synthesis of Zeolite Y Nanocluster. The nano cluster of zeolite Y was synthesized as the following steps [18]. (a) Zeolite Y nanoclusters were prepared by mixing 4.6 g of sodium silicate, 0.9 g of aluminum sulfate, and 1.25 g of sodium hydroxide with 4.8 mL of water while stirring. Then the resulting mixture with a molar ratio of $Na_2O : Al_2O_3 : SiO_2 : H_2O$ at 16 : 1.0 : 15 : 300 was transferred into an autoclave and dynamically aged at 95°C for 24 hours (b) The nanocluster solution obtained in step (a) was added drop wise to a solution obtained by dissolving 0.75 g of TEA-Br in 14.1 mL of water. The pH of the resulting gel was adjusted to 10.5 with a 10% sulfuric acid solution and aged at 45°C for 12 hours. The sample was filtered off, washed with water, and dried at 100°C.

2.3. Preparation of Photocatalyst. 1 g of NaY-zeoilte nanocluster was suspended in 25 mL of distilled water, and magnetically stirred for 6 h. The solution contains 25 mL of 0.05 M $FeSO_4$. The sample was washed with water and collected after filtration. The obtained sample was a fine powder with orange color.

Then, 1 g of exchanged Fe(II) zeolite Y was mixed with 20 mL of 0.1 M o-phenanthroline and stirred for 2 h. The sample was washed with water, collected after filtration, and then the filtrate was dried in air at room temperature. Hereafter, we call zeolite Y nanocluster, Fe(II)-zeolite Y nanocluster and, Fe(II)-O-phenanthrolin-zeolite Y nanocluster as NCY, Fe-NCY, and Fe-OP-NCY, respectively.

2.4. Characterization of Samples. The samples were characterized for phase purity by X-ray diffraction (XRD) (Bruker D8 Advance, CuK_α radiation source). Nanosize property of the synthesized zeolite was distinguished from XRD results using Sherer equation. XRD also was used for structural changes due to incorporation of Fe(II) ions into zeolite structure and complexation of Fe(II) with o-phenanthroline.

FT-IR spectroscopy (Nicolet 400 Impact D) was used to identify structural features and adsorption sites in the NaY samples. All samples were stored in a desiccator until the FT-IR analysis and KBr of spectrometry grade were also heated at 25°C to remove the adsorbed water before pressing. Then 1 mg dried powdered sample was mixed with 100 mg KBr, followed by compressing the mixture to pellets with 12 mm diameter and investigating by the FT-IR spectrometer. Spectra were recorded in a wavenumber region from 400–4000 cm^{-1}. FT-IR also was used for investigation of structural changes due to incorporation of Fe(II) ions into zeolite structure and complexation of Fe(II) with o-phenanthroline. The thermogravimetry (TG) and differential thermogravimetry (DTG) methods were performed for the samples (6 mg) using Model Setaram STA units in the range of 50–800°C with temperature rise of 10°C min^{-1}. The surface morphology of the samples was obtained using a Philips XL30 scanning electron microscope (SEM).

2.5. Photocatalytic Degradation Procedure. The irradiation experiments were carried out in a batch reactor with a 50 mL Flask (Pyrex glass) and UV lamps (75 W). An aqueous catalyst suspension was prepared by adding 50 mg of catalyst powder to a 50 mL solution containing the MG dye at appropriate concentration. For reactions in different pH media, the initial pH of the suspensions was adjusted by addition of either NaOH or HCl solution. Prior to irradiation, the suspensions were magnetically stirred in the dark for 15 minutes to ensure the establishment of adsorption/desorption equilibrium. During the photocatalytic experiments, the slurry composed of dye solution and catalyst was placed in the reactor and stirred magnetically for agitation with simultaneous exposure to visible light. At specific time intervals, samples were withdrawn and to remove the catalyst particles, the solution samples were centrifuged to assess the extent of degradation by UV-Vis spectroscopy.

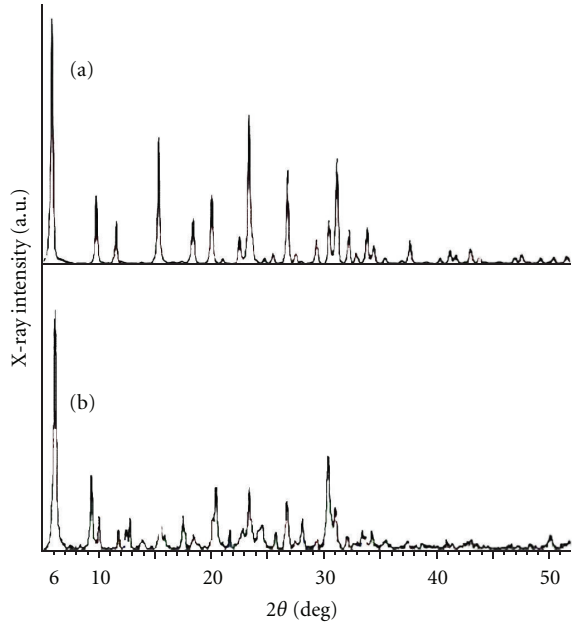

Figure 1: XRD patterns of (a) the pure phase zeolite Y and (b) the pure phase nanozeolite Y.

3. Results and Discussion

3.1. Catalyst Characterization

3.1.1. X-Ray Diffraction Studies. The X-ray diffraction (XRD) patterns of zeolite Y and Na-Y nano cluster are shown in Figures 1(a) and 1(b), respectively. The reflection peaks at 2θ: 6.2, 10.1, 12, 15.8, 20.2, 23.5, and 31 are observed from XRD pattern that show a good agreement with the data of zeolite Na-Y in literature [19] and in the library of the instrument. The XRD pattern of nano cluster has a good conformity with the NaY, except for the presence of broader peaks in nano cluster patterns which show the formation of nano particles during synthesis. This analysis shows that the product has a typical zeolite Y structure.

The X-ray diffraction (XRD) patterns of NCY, Fe-NCY and Fe-OP-NCY samples are shown in Figures 2(a)–2(c), respectively. The XRD pattern of zeolite containing Fe-OP-NCY sample is similar to that of Fe-NCY and the parent NCY, except for a slight change in the intensity of the peaks. These facts confirmed that the framework and crystallinity of zeolite were not destroyed during the preparation. It seems that the relative peak intensities in 2θ of 9.8, 10, and 15.5 reflection are correlated to the location of cations. In zeolite Y, peak intensity is found to decrease in the order: 9.8 > 15.5 > 10, while in encapsulated complexes, the order of peak intensity is as follows: 2θ 15.5 > 9.8 > 10. The difference indicates that the ion-exchange Fe^{2+}, which substitutes at the location of Na^{+}, undergoes rearrangement during complexation [20, 21].

The average particle sizes in powders were calculated by Scherrer's equation using the XRD line broadening method [22]. Crystallite dimensions of zeolites have important implications in intracrystalline diffusion rates of molecules as well as in the contribution of external surface area to adsorption and reaction rates. Over the course of several decades, in both the patent and scientific literature, the Scherrer equation has been applied to estimate the size of zeolite crystallites. The Scherrer equation relates the width of a powder diffraction peak to the average (by volume) dimensions of crystallites in a polycrystalline powder:

$$D = \frac{0.9\lambda}{(B \cdot \cos\theta)}, \tag{1}$$

where D is the crystallite size contribution to the peak width (integral or full width at half maximum) in radians, λ is wavelength of X-ray, B is full width at half maximum, and θ is the diffraction angle [23]. Average particles sizes obtained by Scherrer's equation for NCY, Fe-NCY and Fe-OP-NCY are between 30.5–66.6, 33.5–51.2, and 24.32–58.3 nm, respectively.

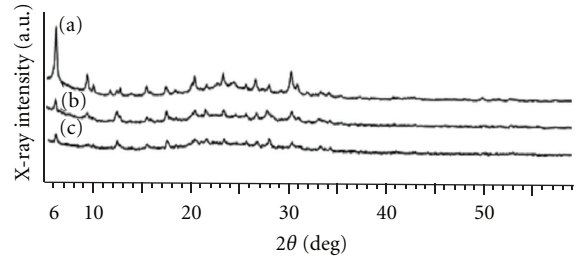

Figure 2: XRD patterns of (a) the NCY, (b) Fe-NCY, and (c) Fe-OP-NCY samples.

3.1.2. FT-IR Studies. FT-IR lattice vibration spectra were used to investigate the influence of incorporation of Fe (II) and Fe(II)-OPhen on the zeolite framework. The FT-IR transmission spectra for zeolite Y, NCY, Fe-NCY, and Fe-OP-NCY are shown in Figure 3. According to Figure 3(a), the observed frequencies at 464, 575, 644, 708, 784, 1001, 1050, 1635 and 3452 cm^{-1} agree with the infrared spectral data, which has been obtained for zeolite Y by Flanigen et al. [24]. The observed frequencies at 469, 574, 798, 1078, 1637, and 3412 cm^{-1} belong to NCY (Figure 3(b)). In comparison with Figures 3(a) and 3(b), changes of the characteristic peaks took place at the right side of the sharp peak at 1001 and 1078 cm^{-1}.

Infrared spectroscopy can reflect the changes in the configuration of the frameworks of the zeolite host, after the incorporation of the guests into the zeolite. Changes of the characteristic peaks took place between the host NCY (the values in the parentheses) and the host-guest materials Fe-NCY and Fe-OP-NCY. For Fe-NCY, the characteristic bands are seen at 467 (469) cm^{-1}, 588 (574) cm^{-1} (T-O bend), 796 (798) cm^{-1} (symmetrical stretch), and 1078 (1078) cm^{-1} (asymmetrical stretch) that show a shift of some bands compared with the bands of the zeolite host (Figures 3(b) and 3(c)). These results can show the incorporation of Fe^{2+} ions into zeolite channels. In addition, the pale yellow color after ion exchange with Fe^{2+} ions is the primary evidence for incorporation of Fe^{2+} into zeolite framework [25].

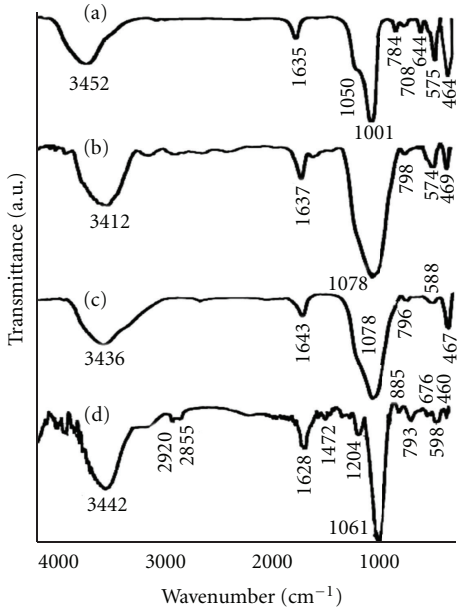

Figure 3: FT-IR spectra of (a) zeolite Y, (b) NCY, (c) Fe-NCY, and (d) Fe-OP-NCY samples.

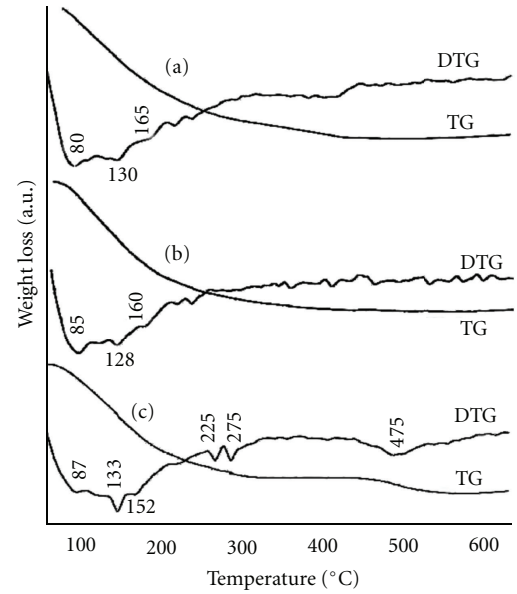

Figure 4: Thermal analysis curves spectra of (a) the NCY, (b) Fe-NCY, and (c) Fe-OP-NCY samples.

A comparison with the spectra of (c) and (d) in Figure 3 shows that the changes have occurred due to conversion of Fe^{2+} ions, to Fe(II)-OPhen. Changes of the characteristic peaks took place between the Fe-NCY (the values in the parentheses) and Fe-OP-NCY. For Fe-OP-NCY, the characteristic bands are seen at 460 (467) cm^{-1}, 598 (588) cm^{-1}, 793 (796) cm^{-1}, 1061 (1078) cm^{-1}, and 1628 (1643) cm^{-1} that show a shift of some bands compared to the bands of the Fe-NCY. In addition, there are some peaks at 676, 1204, 1472, 2855, and 2920 cm^{-1} in Fe-OP-NCY spectrum that are absent in Fe-NCY spectrum. Changes in Fe-OPh-NCY spectrum are different from the other spectra. These results demonstrate that the guest Fe-OPhen incorporated into the NCY had some interactions with the inner surfaces of the zeolite host at the same time. The spectra of all of the Fe(II) complexes are dominated by bands between ~2980 cm^{-1} due to υ (Alph.-CH) groups. A new band appearing in the ~1200 cm^{-1} region was assigned to υ(R-O) mode. The stretching vibration υ (Ar-C=C) shows a bands in the ~1427 cm^{-1} range. Conclusive evidence of the bonding is also shown that bands in the IR spectra of the Fe(II) complexes appear at ~460 cm^{-1} assigned to υ(Fe-O) stretching vibration [26]. The obtained product after complexation process shows a change in color from pale yellow to orange that in turn can show conversion of Fe^{2+} to Fe(II)-Ophen in the zeolite.

Generally, acidity of a framework increases with increasing of M^{2+} substitution, but there was no obvious trend in the absorption bands assigned to terminal hydroxyl groups (3734 cm^{-1}) or to the absorption bands assigned to bridging hydroxyl groups associated with a Bronsted site (3650–3600 cm^{-1}) [27, 28].

3.1.3. Thermal Analysis Studies. The TG and DTG curves for NCY, Fe-NCY, and Fe-OP-NCY are shown in Figure 4. Water is lost in three steps for NCY, Fe-NCY, and Fe-OP-NCY. The peaks at 80, 130, and 165°C (Figure 4(a)), 85, 128, and 160°C (Figure 4(b)) and, 87, 133, and 151°C (Figure 4(c)) are seen in the DTG curves.

The thermal decomposition of Fe-OP-NCY through endothermic peak at 225 and 275°C, corresponding to the release of Orthophenanthrolin ligand, remained due to incomplete washing of the zeolite after preparation of Fe-OP-NCY [29]. The endothermic loss occurs in a wide temperature range (450–700°C) and is due to the slow decomposition of the chelating ligand. The DTG results for Fe-OP-NCY are similar to literature [29, 30]. The weight loss percent for NCY, Fe-NCY, and Fe-OP-NCY samples was obtained 8.3, 8.2, and 9.2%, respectively.

3.1.4. SEM Analysis. The surface morphology of zeolite Y, Fe-NCY, and Fe-OP-NCY has been studied by scanning electron microscopy. The SEM pictures of the unloaded zeolite and samples are presented in Figure 5. The crystallites of the unloaded zeolite, with size about 90 nm, have a very well-defined spherical grain-like crystals. The image of the loaded samples also shows the spherical crystals that indicates that the zeolite crystallites are not affected by the Fe and Fe-OP loading. The average particle size of Fe-NCY and Fe-OP-NCY samples is about 50–78 and 63–87 nm respectively.

3.2. Photocatalytic Decolorization of MG by F-OP-NCY. After characterizing of the Fe-OP-NCY, the obtained material was used for the photocatalytic decolorization of a 40 ppm MG dye solution containing 1 g L^{-1} photoctalyst under UV irradiation at varied conditions. A negligible decrease in the concentration of dye was observed under irradiation in the absence of photocatalyst or in the presence of photocatalyst without a light source. It is evident from the following results that the photolysis of the MG solution in the presence of

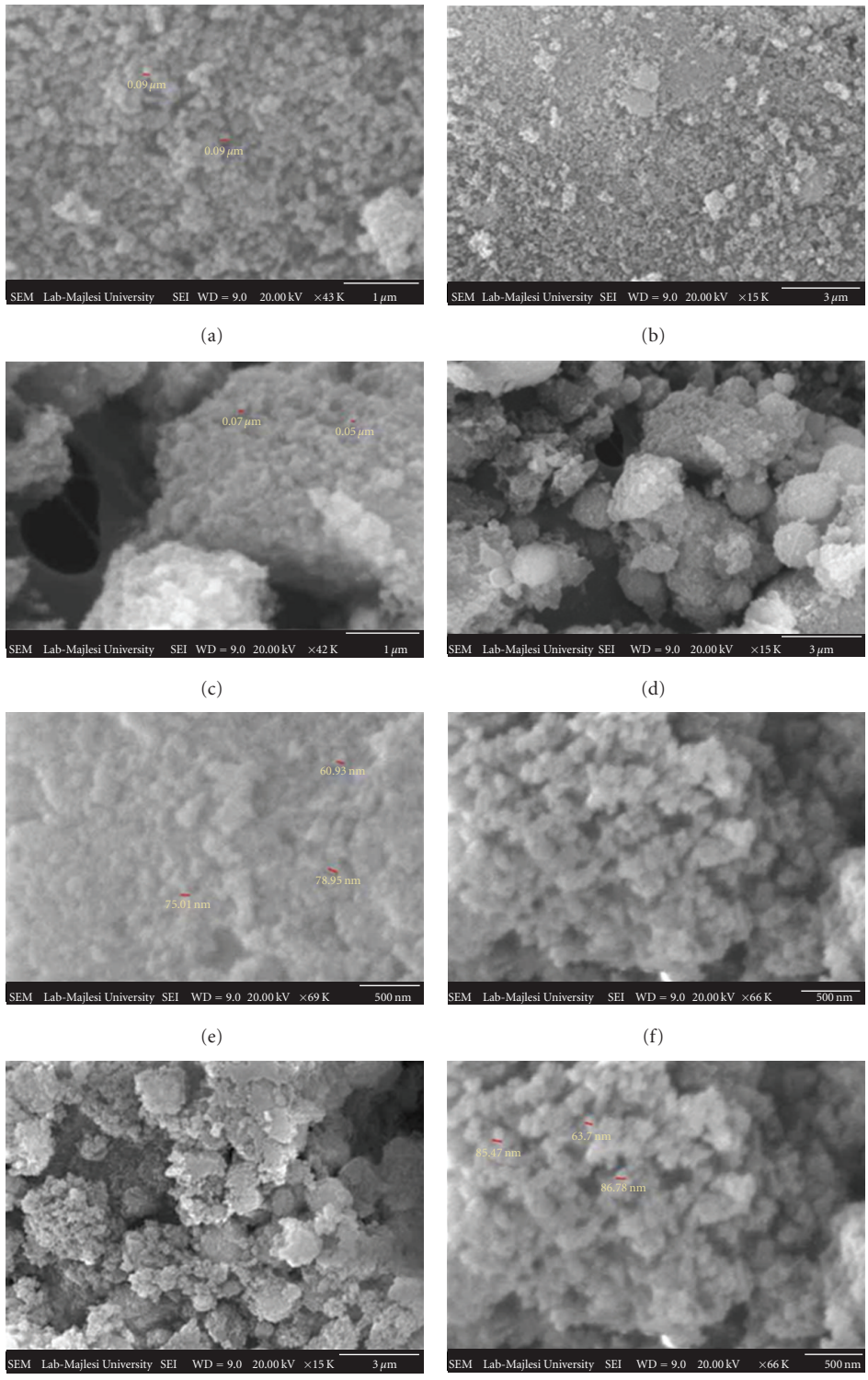

Figure 5: SEM images of (a, b) the NCY, (c–e) Fe-NCY, and (f–h) Fe-OP-NCY samples.

photocatalyst leads to the disappearance of the compound. On the other hand, the blank experiments either with illuminating MG or with the suspension containing photocatalyst and MG in the dark showed that both illumination and the catalyst were necessary for the destruction of the dye.

3.2.1. Effect of Catalyst Concentration. The initial rate of photocatalytic degradation of many pollutants is a function of the photocatalyst dosage [31]. A series of experiments was performed to assess the optimum catalyst loading by varying the amount of catalyst from 0.7 to 8.0 g L^{-1} using a 40 ppm

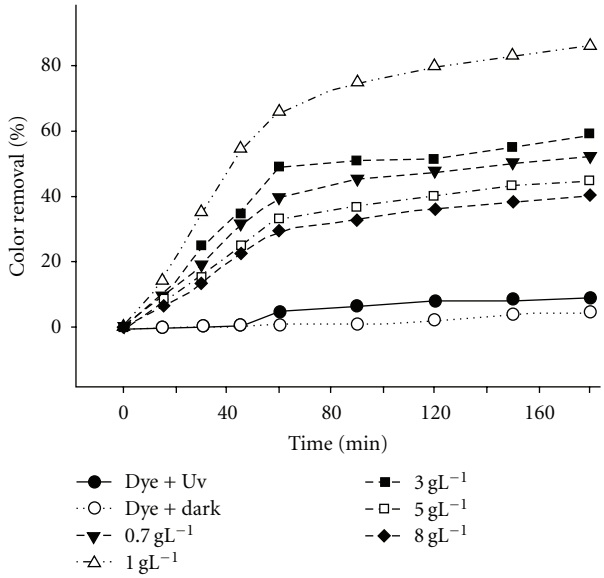

Figure 6: The effects of photocatalyst concentration on the photodecolorization of methyl green [methyl green]$_0$ = 40 mg L^{-1}, pH = 5.2, T = 25°C.

methyl green solution. The depicted results in Figure 6 exhibit that the degradation rate increases with increasing the mass of catalyst, reached the higher value (1 g L^{-1} of the catalyst), and then decreased considerably. The reason for this decrease can be the fact that when the concentration of the catalyst rises, the solid particles increasingly block the penetration of the photons. So the overall number of the photons that can be reached to catalyst particles and the production of OH radicals decreased with the loading of the catalyst [32]. Another reason may be due to the aggregation of solid particles while a large amount of catalyst is used [32, 33]. Figure 6 also shows that the removal rates were negligible in the absence of catalyst or dark conditions after 3 hour control.

Many authors have reported that the kinetic behavior of photocatalytic reactions obeys first-order reaction [31, 33]. In order to confirm the speculation, $\ln(C/C_0)$ was plotted as a function of the irradiation time. The calculated results indicated that the first-order model gives a better fit. The rate constant values, k (min^{-1}), were calculated from the straight-line portion of the first-order plots as a function of the catalyst mass and are listed in Table 1. As the results show, maximum degradation (80%) of MG dye was observed after 120 min with the maximum rate constant (7.6×10^{-2} min^{-1}) in the presence of 1 g L^{-1} of the catalyst. Methyl green alone could not be transformed under UV irradiation, corresponding to the rate constant (k) of 1.16×10^{-5} min^{-1}. In the next experiments, 1 g L^{-1} of Fe-OP-NCY was used as the optimum dosage.

3.2.2. Effect of Methyl Green Concentration. The degradation efficiency also depends on the initial concentration of the substrate [34]. The MG decolorization was studied over the concentration range of 20–100 ppm by maintaining the other parameters constant. The decolorization is highest at 40 ppm and thereafter decreases (Figure 7). The lifetimes of hydroxyl radicals are very short (only a few nanoseconds) and thus they can only react where they formed. Increasing the quantity of MG molecules per volume unit logically enhances the probability of collision between organic matter and oxidizing species, leading to an increase in the degradation efficiency. It is seen that the degradation efficiency of dye decreased when increasing the initial concentration to more than 40 ppm. With increasing the amounts of dye to more than 40 ppm, more of dye molecules will be adsorbed on the surface of the photocatalyst and the active sites of the catalyst will be reduced. On the other hand, as the dye concentration increases, the equilibrium adsorption of dye at the active sites of the catalyst surface increases; hence competitive adsorption of O_2 and OH^- at the same sites decreases, that causes a lower formation rate of $O_2^{\bullet -}$ and $^{\bullet}OH$ radicals which are necessary for high degradation efficiency. According to the Beer-Lambert law, as the initial dye concentration increases, the path length of photons entering the solution decreases, that causes lower photon absorption on catalyst particles and consequently a lower photodegradation rate. Also, with increasing of the dye concentration some of the photons are absorbed by molecules of the dye and the excitation of photocatalyst particles by photons will be reduced. These results are in good accordance with the literature [33–38]. This is also simplified in Table 1 where the degradation rate constant (k, min^{-1}) is listed as a function of initial concentration of the dye.

Table 1: Reaction rate constant of MG photodecolorization as a function of various experimental parameters.

Parameter	Value	$k \times 100$ (min^{-1})
Photocatalyst mass (g L^{-1})	a	0.011
	b	0.15
	0.7	4.4
	1.0	8.9
	3.0	5.1
	5.0	3.1
	8.0	2.9
MG concentration (ppm)	20	8.2
	40	9.1
	60	2.8
	80	1.3
	100	1.2
pH	3.6	5.666×10^{-6}
	5.2	9.2
	7.1	10.8
	9.3	19.3
Temperature (°C)	25	7.8
	40	8.8
	50	10.4
	60	9.3

[a]The proposed process was performed in the dark condition and in the presence of the Fe-OP-NCY to investigate the surface adsorption extent.
[b]The photolysis extent was determined at the absence of the Fe-OP-NCY under UV irradiation.

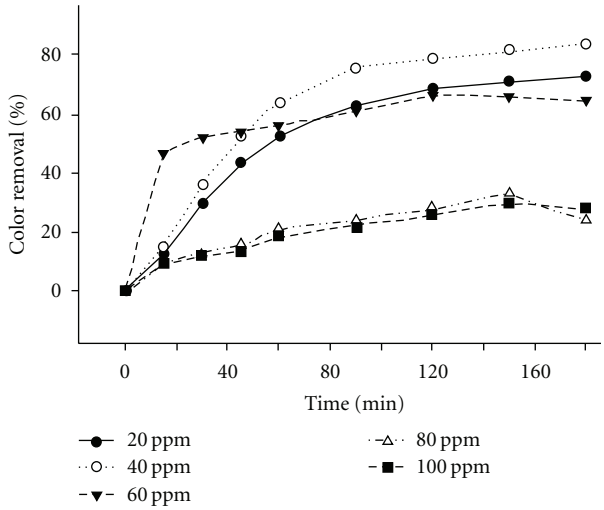

Figure 7: The effect of dye concentration on the photodegradation methyl green [Fe-OP-NCY] = 1 g L^{-1}, pH = 5.2, T = 25°C.

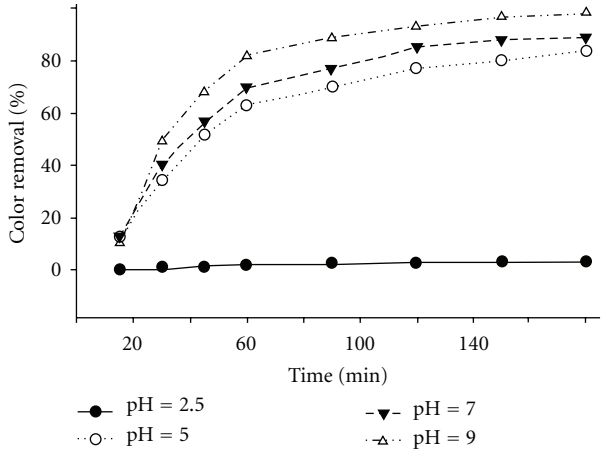

Figure 8: pH dependence of methyl green decolorization in irradiated solutions [methyl green]$_0$ = 40 mg L^{-1}, [Fe-OP-NCY] = 1 g L^{-1}, T = 25°C.

3.2.3. Effect of pH. Wastewaters from the textile industries usually have a wide range of pH values. Generally pH plays an important role in both characteristics of textile wastes and generation of active sites [38, 39]. Hence, the role of pH on the percentage of degradation was studied in the pH range of 3–9 using a 40 ppm methyl green solution and 1 g L^{-1} of the catalyst. The solution pH was adjusted only prior to irradiation and was not controlled during the reaction. Figure 8 shows that the percentage of decolorization increases with increasing of pH. As it is mentioned in the literature [34], in the initial acidic pH, concomitant with acidification of the solution by HCl, a high amount of conjugated base is added to the solution. The anion Cl^- is able to react with hydroxyl radicals leading to inorganic radical ions ($ClO^{-\bullet}$). These inorganic radical anions show a much lower reactivity than $^{\cdot}OH$, so that they do not take part in the dye degradation. There is also a drastic competition between the dye and anions with respect to $^{\cdot}OH$. Hence, increasing

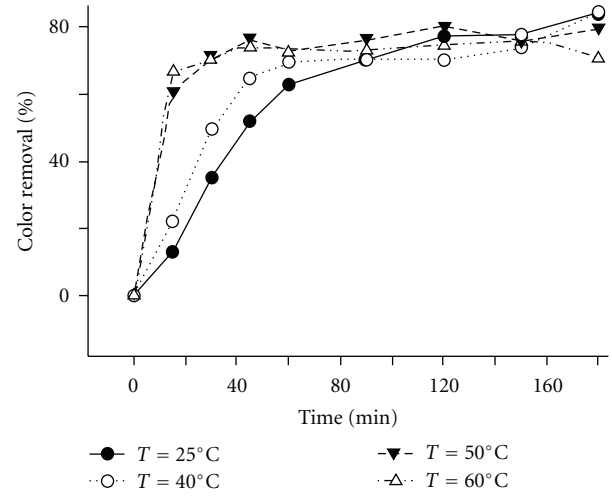

Figure 9: The effects of temperature on the photodegradation methyl green [methyl green]$_0$= 40 mg L^{-1}, [Fe-OP-NCY] = 1 g L^{-1}, pH = 5.2.

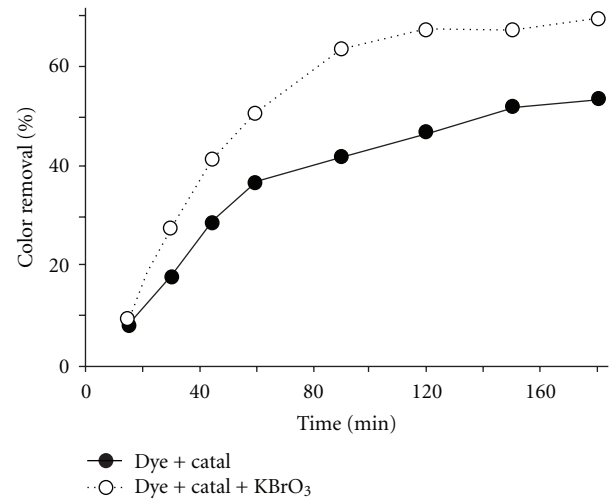

Figure 10: The effects of electron acceptor on the photodegradation methyl green [methyl green]$_0$ = 40 mg L^{-1}, [Fe-OP-NCY] = 1 g L^{-1}, pH = 5.2, [$KBrO_3$] = 20 mg L^{-1}.

in pH shows an increasing in degradation efficiency. In alkaline pHs, the presence of a large quantity of OH^- ions causes the formation of more OH radicals, which enhances the photocatalytic degradation of MG significantly [40]. In acidic solutions a decrease of the decolorization rate was observed reflecting the difficulty of the dye molecules to approach the catalyst surface due to electrostatic interaction. In other words, at low pH, the adsorption of cationic dye on the surface of photocatalyst decreases because the photocatalyst surface will be positively charged and repulsive force is increased due to decreasing adsorption [33]. The rate constant values (k, min^{-1}) as a function of pH on the dye degradation are presented in Table 1.

3.2.4. Effect of Temperature. Since the photonic activation occurs at considerably high speeds, it is expected that

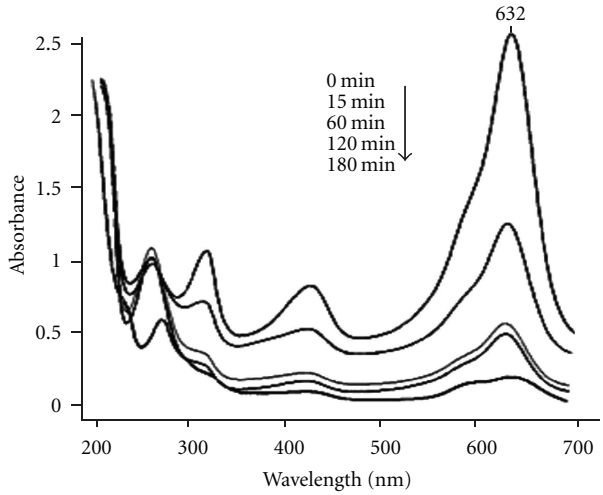

FIGURE 11: Decrease absorption spectra of MG (40 mg L^{-1} dye solution, pH = 5.2) in the presence of photocatalyst (1 g L^{-1}) in time interval of 180 min.

the photocatalytic system is not sensible to the temperature, and the true activation energy must be then equal to zero. Although considering that the reactions under study occur preferentially in the liquid/solid interface, a nonzero value must be expected as apparent activation energy. With the increase of temperature, the exothermic adsorption of the reactants becomes disfavored due to reducing the value of the apparent activation energy [41]. It was observed that with increasing the temperature from 25 to 60°C (using a 40 ppm MG solution and 1g $L^{-1}$of the catalyst), the percentage of decolorization increases (Figure 9). The rise in the temperature shows that it is effective at the initial stages of the process. It has reported that an increase in temperature helps the reaction to compete more effectively with e^-_{cb} − h^+_{vb} recombination [42]. On the other hand, an increase in temperature decreases the solubility of oxygen in water which is not desirable. Higher temperatures will cause significant evaporation of the solution during the experiments. Thus, temperature higher than 50°C is not recommended. The rate constant values (k, min^{-1}) as a function of temperature on the dye degradation are presented in Table 1.

3.2.5. Effects of Electron Acceptor. Electron accepters such as H_2O_2, $(NH_4)_2S_2O_8$, and $KBrO_3$ can influence on photodegradtion efficiency [43, 44]. The role of $KBrO_3$ (20 ppm) on the degradation rate of MG was studied at a pH of 5.2 (initial pH of the solution), using a 40 ppm of the dye solution, 1 g L^{-1} of catalyst, and 3 hour irradiation. The dye degradation in the presence of the above electron accepter after 180 min is shown in Figure 10. The results show that the rate of degradation enhances in the presence of $KBrO_3$. The pronounced effect of bromate ion on MG degradation may be due to the change of reaction mechanism, since the reduction of bromate ions by electrons does not directly form hydroxyl radicals, but form other oxidizing species like BrO_2^- and HOBr. Furthermore bromate ions by themselves can act as oxidizing agents [45].

3.3. UV-Vis Studies. Figure 11 shows the decolorization of MG dye (40 ppm) under irradiation in time interval of 180 min and in the presence of catalyst (1 g L^{-1}, pH = 5.2). The decrease of the sample's absorbance intensity at its λ_{max} is indicated by the decolorization of the dye in the applied conditions. As a consequence the decrease of samples absorbance due to decrease of the dye concentration was recorded for measurement of decolorization rate in all abovementioned parameters. Since there are no additional peaks appearing in the UV-Vis spectra, the dye is completely degraded. According to UV-Vis spectra we suggest that the products of the decolorization process are H_2O, CO_2, NO_2 and SO_3. The proposed mechanism for dye decolorization using photocatalyst (PC) is suggested as follows [2, 14, 34, 35, 37, 40, 44]:

$$\begin{aligned}
PC + hv &\longrightarrow h^+_{vb} + e^-_{cb}\\
OH^- + h^+_{vb} &\longrightarrow {}^\bullet OH\\
H_2O + h^+_{vb} &\longrightarrow {}^\bullet OH + H^+\\
O_2 + e^-_{cb} &\longrightarrow O_2^{-\bullet}\\
O_2^{-\bullet} + e^-_{cb} + 2H^+ &\longrightarrow H_2O_2 \qquad (2)\\
2O_2^{-\bullet} + 2H^+ &\longrightarrow O_2 + H_2O_2\\
H_2O_2 + e^-_{cb} &\longrightarrow OH^- + {}^\bullet OH\\
Dye + h^+_{vb} &\longrightarrow Dye^{+\bullet} \longrightarrow \text{Final products}\\
Dye + {}^\bullet OH &\longrightarrow Dye^\bullet \longrightarrow \text{Final products.}
\end{aligned}$$

4. Conclusion

The results obtained clearly show that when an Fe-O-Phenanthroline complex is loaded on zeolite Y nano cluster, the obtained composite shows a photocatalytic effect in decolorization of MG dye under UV irradiation. The photocatalytic degradation efficiency of methyl green (MG) was achieved up to 80% during 120 min. It is important to choose the optimum degradation parameters for increasing the degradation rate. $KBrO_3$ as an electron acceptor increased the efficiency of the dye degradation. The results showed that the proposed degradation process is a heterogeneous process, so Fe(II)-*O*-phenanthroline as dissolved in the solution (homogeneous phase) did not show considerable degradation efficiency.

References

[1] *Ullmann's Encyclopedia of Industrial Chemistry*, vol. 27, John Wiley & Sons, Hoboken, NJ, USA, 2001.

[2] D. P. Duxbury, "The photochemistry and photophysics of triphenylmethane dyes in solid and liquid media," *Chemical Reviews*, vol. 93, no. 1, pp. 381–433, 1993.

[3] T. Inoue, K. Kikuchi, K. Hirose, M. Iino, and T. Nagano, "Small molecule-based laser inactivation of inositol 1,4,5-trisphosphate receptor," *Chemistry and Biology*, vol. 8, no. 1, pp. 9–15, 2001.

[4] B. G. Berg and D. M. Green, "Spectral weights in profile listening," *Journal of the Acoustical Society of America*, vol. 88, no. 2, pp. 758–766, 1990.

[5] T. Geethakrishnan and P. K. Palanisamy, "Degenerate four-wave mixing experiments in Methyl green dye-doped gelatin film," *Optik*, vol. 117, no. 6, pp. 282–286, 2006.

[6] J. M. Joseph, R. Varghese, and C. T. Aravindakumar, "Photoproduction of hydroxyl radicals from Fe(III)-hydroxy complex," *Journal of Photochemistry and Photobiology A*, vol. 146, no. 1-2, pp. 67–73, 2001.

[7] J. Šubrt, J. M. Criado, L. Szatmáry et al., "Mechanochemical synthesis of visible light sensitive titanium dioxide photocatalyst," *International Journal of Photoenergy*, vol. 2011, Article ID 156941, 9 pages, 2011.

[8] J. C. Jansen, M. Stocker, H. G. Karge, and J. Weitkamp, Eds., *Advanced Zeolite Science and Applications*, Elsevier Science, New York, NY, USA, 1994.

[9] N. Herron and D. R. Corbin, *Inclusion Chemistry with Zeolites: Nanoscopic Materials by Design*, Kluwer Academic Publishers, Dordrechet, The Netherlands, 1995.

[10] M. C. Dalconi, A. Alberti, G. Cruciani, P. Ciambelli, and E. Fonda, "Siting and coordination of cobalt in ferrierite: XRD and EXAFS studies at different Co loadings," *Microporous and Mesoporous Materials*, vol. 62, no. 3, pp. 191–209, 2003.

[11] M. S. Orensen, F. H. Frimmel, and Z. Naturforch, "Homogeneous photocatalysis by transition metal complexes in the environment," *Journal of Molecular Catalysis A*, vol. 224, pp. 17–33, 2004.

[12] F. G. Kari, S. Hilger, and S. Canonica, "Determination of the reaction quantum yield for the photochemical degradation of Fe(III)—EDTA: implications for the environmental fate of EDTA in surface waters," *Environmental Science and Technology*, vol. 29, no. 4, pp. 1008–1017, 1995.

[13] H. D. Burrows, M. Canle L, J. A. Santaballa, and S. Steenken, "Reaction pathways and mechanisms of photodegradation of pesticides," *Journal of Photochemistry and Photobiology B*, vol. 67, no. 2, pp. 71–108, 2002.

[14] P. Boule, M. Bolte, R. Richard, and C. Richard, "Auto-remediation of surface waters by solar-light: photolysis of 1-naphthol, and two herbicides in pure and synthetic waters," in *Environmental Photochemistry*, P. Boule, M. Bolte, R. Richard, and P. Boule, Eds., p. 181, Springer, Berlin, Germany, 1999.

[15] H. Kawaguchi and A. Inagaki, "Photochemical generation rates of hydroxyl radical in aqueous solutions containing Fe(III)-hydroxy complex," *Chemosphere*, vol. 27, no. 12, pp. 2381–2387, 1993.

[16] J. M. Joseph, R. Varghese, and C. T. Aravindakumar, "Photoproduction of hydroxyl radicals from Fe(III)-hydroxy complex: a quantitative assessment," *Journal of Photochemistry and Photobiology A*, vol. 146, no. 1-2, pp. 67–73, 2001.

[17] J. Sima and J. Makanova, "Photochemistry of iron (III) complexes," *Coordination Chemistry Reviews*, vol. 160, pp. 161–189, 1997.

[18] Q. Tan, X. Bao, T. Song et al., "Synthesis, characterization, and catalytic properties of hydrothermally stable macro-meso-micro-porous composite materials synthesized via in situ assembly of preformed zeolite Y nanoclusters on kaolin," *Journal of Catalysis*, vol. 251, no. 1, pp. 69–79, 2007.

[19] H. Robson, "Verified synthesis of zeolitic materials," *Microporous and Mesoporous Materials*, vol. 22, pp. 551–666, 1998.

[20] M. Salavati-Niasari, Z. Salimi, M. Bazarganipour, and F. Davar, "Synthesis, characterization and catalytic oxidation of cyclohexane using a novel host (zeolite-Y)/guest (binuclear transition metal complexes) nanocomposite materials," *Inorganica Chimica Acta*, vol. 362, no. 10, pp. 3715–3724, 2009.

[21] M. Salavati-Niasari, "Template synthesis and characterization of host (nanopores of zeolite Y)/guest (Co(II)-tetraoxodithiatetraaza macrocyclic complexes) nanocomposite materials," *Polyhedron*, vol. 27, no. 15, pp. 3207–3214, 2008.

[22] V. Uvarov and I. Popov, "Metrological characterization of X-ray diffraction methods for determination of crystallite size in nano-scale materials," *Materials Characterization*, vol. 58, no. 10, pp. 883–891, 2007.

[23] A. W. Burton, K. Ong, T. Rea, and I. Y. Chan, "On the estimation of average crystallite size of zeolites from the Scherrer equation: a critical evaluation of its application to zeolites with one-dimensional pore systems," *Microporous and Mesoporous Materials*, vol. 117, no. 1-2, pp. 75–90, 2009.

[24] E. M. Flanigen, H. Khatami, and H. A. Szymanski, *Molecular Sieve Zeolites*, vol. 101 of *Advances in Chemistry Series*, American Chemical Society, Washington, DC, USA, 1971.

[25] M. S. Nahar, K. Hasegawa, S. Kagaya, and S. Kuroda, "Adsorption and aggregation of Fe(III)-hydroxy complexes during the photodegradation of phenol using the iron-added-TiO_2 combined system," *Journal of Hazardous Materials*, vol. 162, no. 1, pp. 351–355, 2009.

[26] M. Salavati-Niasari, "Nanodimensional microreactors encapsulation of 15- and 16-membered diaza dioxa macrocyclic Schiff-base copper(II) complex nanoparticles: synthesis and characterization," *Inorganic Chemistry Communications*, vol. 13, no. 2, pp. 266–272, 2010.

[27] A. Dyer, *An Introduction to Zeolite Molecular Sieves*, John Wiley & Sons, Chichester, UK, 1988.

[28] D. A. Skoog and J. J. Leary, *Principles of Instrumental Analysis*, Saunders College Publishing, New York, NY, USA, 4th edition, 1992.

[29] M. Salavati-Niasari, "Template synthesis and characterization of hexaaze macrocycles containing pyridine iron(II) complex nanoparticles dispersed within nanireacrors of zeolite-Y," *Inorganic Chemistry Communications*, vol. 12, pp. 359–363, 2009.

[30] B. M. Kukovec, Z. Popovic, B. Kozlevčar, and Z. Jagličić, "3D supramolecular architectures of copper(II) complexes with 6-methylpicolinic and 6-bromopicolinic acid: synthesis, spectroscopic, thermal and magnetic properties," *Polyhedron*, vol. 27, no. 18, pp. 3631–3638, 2008.

[31] M. H. Habibi, M. Nasr-Esfahani, and T.A. Egerton, "Photochemical characterization and photocatalytic properties of a nanostructure composite TiO2 film, internat," *International Journal of Photoenergy*, vol. 2007, Article ID 13653, 8 pages, 2007.

[32] M. S. Lucas and J. A. Peres, "Decolorization of the azo dye Reactive Black 5 by fenton and photo-Fenton oxidation," *Dyes and Pigments*, vol. 71, no. 3, pp. 236–244, 2006.

[33] H. R. Pouretedal, A. Norozi, M. H. Keshavarz, and A. Semnani, "Nanoparticles of zinc sulfide doped with manganese, nickel and copper as nanophotocatalyst in the degradation of organic dyes," *Journal of Hazardous Materials*, vol. 162, no. 2-3, pp. 674–681, 2009.

[34] A. N. Ejhieh and M. Khorsandi, "Photodecolorization of Eriochrome Black T using NiS-P zeolite as a heterogeneous catalyst," *Journal of Hazardous Materials*, vol. 176, no. 1–3, pp. 629–637, 2010.

[35] A. Nezamzadeh-Ejhieh and S. Hushmandrad, "Solar photodecolorization of methylene blue by CuO/X zeolite as a heterogeneous catalyst," *Applied Catalysis A*, vol. 388, no. 1-2, pp. 149–159, 2010.

[36] Z. M. El-Bahy, M. M. Mohamed, F. I. Zidan, and M. S. Thabet, "Photo-degradation of acid green dye over Co-ZSM-5

catalysts prepared by incipient wetness impregnation technique," *Journal of Hazardous Materials*, vol. 153, no. 1-2, pp. 364–371, 2008.

[37] A. Nezamzadeh-Ejhieh and S. Moeinirad, "Heterogeneous photocatalytic degradation of furfural using NiS-clinoptilolite zeolite," *Desalination*, vol. 273, pp. 248–257, 2011.

[38] K.M. Parida, N. Baliarsingh, B. Sairam Patra, and J. Das, "Copper phthalocyanine immobilized Zn/Al LDH as photocatalyst under solar radiation for decolorization of methylene blue," *Journal of Molecular Catalysis A*, vol. 267, pp. 202–208, 2007.

[39] H. R. Pouretedal, H. Eskandari, M. H. Keshavarz, and A. Semnani, "Photodegradation of organic dyes using nanoparticles of cadmium sulfide doped with manganese, nickel and copper as nanophotocatalyst," *Acta Chimica Slovenica*, vol. 56, no. 2, pp. 353–361, 2009.

[40] A. Nezamzadeh-Ejhieh and M. Khorsandi, "Heterogeneous photodecolorization of Eriochrome Black T using Ni/P zeolite catalyst," *Desalination*, vol. 262, pp. 79–85, 2010.

[41] A. E. H. Machado, J. A. Miranda, R. F. Freitas et al., "Destruction of the organic matter present in effluent from a cellulose and paper industry using photocatalysis," *Journal of Molecular Catalysis A*, vol. 155, pp. 231–241, 2003.

[42] J. Saien and A. R. Soleymani, "Degradation and mineralization of Direct Blue 71 in a circulating upflow reactor by UV/TiO_2 process and employing a new method in kinetic study," *Journal of Hazardous Materials*, vol. 144, no. 1-2, pp. 506–512, 2007.

[43] A. K. Gupta, A. Pal, and C. Sahoo, "Photocatalytic degradation of a mixture of Crystal Violet (Basic Violet 3) and Methyl Red dye in aqueous suspensions using Ag_+ doped TiO_2," *Dyes and Pigments*, vol. 69, no. 3, pp. 224–232, 2006.

[44] U. I. Gaya and A. H. Abdullah, "Heterogeneous photocatalytic degradation of organic contaminants over titanium dioxide: a review of fundamentals, progress and problems," *Journal of Photochemistry and Photobiology C*, vol. 9, no. 1, pp. 1–12, 2008.

[45] M. Saquib and M. Muneer, "Photocatalytic degradation of two selected textile dye derivatives, eosine yellowish and p-rosaniline, in aqueous suspensions of titanium dioxide," *Journal of Environmental Science and Health, Part A*, vol. 38, no. 11, pp. 2581–2598, 2003.